Journal of Power Sources 196 (2011) 7700–7706

Contents lists available at ScienceDirect

Journal of Power Sources

journal homepage: www.elsevier.com/locate/jpowsour

Lithium bis(fluorosulfonyl)imide–$PYR_{14}TFSI$ ionic liquid electrolyte compatible with graphite

Martina Nádherná[a,b], Jakub Reiter[a,*], Jože Moškon[c,d], Robert Dominko[c,d]

[a] Institute of Inorganic Chemistry of the ASCR, v.v.i., 250 68 Řež near Prague, Czech Republic
[b] Department of Analytical Chemistry, Faculty of Science, Charles University in Prague, Albertov 2030, 128 40 Prague 2, Czech Republic
[c] National Institute of Chemistry, Hajdrihova 19, SI-1000 Ljubljana, Slovenia
[d] CO-NOT Centre of Excellence, Hajdrihova 19, SI-1000 Ljubljana, Slovenia

ARTICLE INFO

Article history:
Received 20 February 2011
Received in revised form 5 April 2011
Accepted 17 April 2011
Available online 23 April 2011

Keywords:
Graphite
Ionic liquid
Bis(fluorosulfonyl)imide
Lithium-ion battery
Solid electrolyte interface

ABSTRACT

Lithium bis(fluorosulfonyl)imide (LiFSI) in 1-butyl-1-methylpyrrolidinium bis(trifluoromethanesulfonyl)imide ($PYR_{14}TFSI$) was successfully tested as an electrolyte for graphite composite anodes at elevated temperature of 55 °C. The graphite anode showed a good cyclability during the galvanostatic testing at C/10 rate and 55 °C with the capacity close to theoretical. The formation of SEI in different electrolytes was the subject of study using impedance spectroscopy on symmetrical cells containing two lithium electrodes. The 0.7 m LiFSI in $PYR_{14}TFSI$ exhibits a good ionic conductivity (5.9 mS cm^{-1} at 55 °C) along with high electrochemical stability and high thermal stability. These properties allow their potential application in large-scale lithium ion batteries with improved safety.

© 2011 Elsevier B.V. All rights reserved.

1. Introduction

Recent large-scale application of lithium-ion batteries requires high device safety standards and low impact on human health and environment. The main source of risk in the lithium-ion battery is connected with present organic electrolyte based on volatile and flammable organic solvents and lithium hexafluorophosphate that is highly toxic, easily degradable by water moisture and reacts with carbonates forming poisonous compounds such as hydrogen fluoride and fluorinated organic compounds (e.g. 1-fluoro-2-(2-fluoroethoxy)ethane) [1,2].

A substantial safety improvement can be achieved by using room temperature ionic liquids as the main component of the electrolyte [3,4]. Many papers have been published on the compatibility of various cathodic materials ($LiCoO_2$, $LiMn_2O_2$, $LiFePO_4$, Li_2FeSiO_4) with ionic liquids [5–7,8], but the stability of ionic liquids at low potentials is problematic particularly in the case of disubstituted imidazolium-based representatives [9] and remains a challenge at the current state of research.

A possible solution can be the use of titanium oxide based electrode material as anode [10], which, compared to the system with graphite, is associated with a decrease of energy density. The use of carbonaceous-based anode material requires ionic liquids with electrochemically stable organic cation. The tri-substituted imidazolium-based ionic liquids (1-propyl-2,3-dimethylimidazolium and 1-butyl-2,3-dimethylimidazolium) are chemically stable with metallic lithium [11]. The substitution of the H-2 hydrogen atom on the imidazolium ring improves the electrochemical stability from 0.9–1.0 to 0.5 V vs. Li/Li$^+$, but below 0.5 V the ionic liquids (both PMMI TFSI and BMMI TFSI) undergo an irreversible reduction on platinum [12,13].

The most stable ionic cations from the family of nitrogen-based ionic liquids are the quaternary aliphatic or alicyclic cations such as N,N,N-trimethyl-N-hexylammonium [14], N,N-diethyl-N-methyl-N-(2-methoxyethyl)ammonium [15], N-methyl-N-alkylpyrrolidinium and N-methyl-N-alkylpiperidinium [16]. The ionic liquids based on quaternary nitrogen are stable even at the potential of metallic lithium, what allows the electrochemical plating and stripping of metallic lithium from these electrolytes [17].

Despite the improved stability of some ionic liquids at low potentials, graphite is not compatible with most of them due to intercalation of the organic cation between the graphene layers [18]. The solution is using SEI-forming agents such as vinylene carbonate [19–21], vinyl ethylene carbonate [22], fluoroethylene carbonate [9], chlorethylene carbonate [23], ethylene sulfite [24] as additives responsible for the SEI formation via electrochemical reduction-polymerisation.

* Corresponding author. Tel.: +420 266172198; fax: +420 220941502.
E-mail address: reiter@iic.cas.cz (J. Reiter).

0378-7753/$ – see front matter © 2011 Elsevier B.V. All rights reserved.
doi:10.1016/j.jpowsour.2011.04.033

The introduction of bis(fluorosulfonyl)imide anion FSI^- [25,26] in a PEO-based polymer gel electrolyte showed that FSI^- can act as a SEI-forming agent for carbonaceous anodes and, at the same time, can form numerous ionic liquids with low viscosity and high conductivity such as EMI FSI, $PYR_{13}FSI$ or $PYR_{14}FSI$ [27]. These ionic liquids have been successfully tested as the main electrolyte component for graphite-based anodes [7,28–33]. Nevertheless, the FSI-based ionic liquids showed a lower electrochemical stability window than the TFSI analogues [32] and slightly worse safety properties with charged electrode materials [34] and a higher production cost.

In this work, we evaluate the compatibility and the electrochemical performance of electrolyte solutions based on 1-butyl-1-methylpyrrolidinium bis(trifluoromethanesulfonyl)imide ($PYR_{14}TFSI$) and lithium bis(fluorosulfonyl) imide (LiFSI). The advantage over the previously used FSI-based electrolytes is a lower content of the FSI^- anion (neat $PYR_{14}FSI$ ionic liquid was found unsuitable for the graphite electrode [32,33]).

Our focus is in optimisation of ionic liquid-based electrolyte solutions compatible with graphite at 55 °C that can be further used with selected cathode material that require a higher long-term operational temperature.

2. Experimental

2.1. Synthesis of ionic liquids and LiFSI, preparation of electrolytes

The method of preparation is based on a two-step synthesis, when bromide ($PYR_{14}Br$) is prepared by direct alkylation of 1-methylpyrrolidine and then substituted with bis(trifluoromethanesulfonyl)imide in an aqueous solution. Considering the environmental requirements, the method of ionic liquid preparation is based on a direct synthesis eliminating the use of either a large excess of either alkylbromide or halogenated solvents in both synthetic steps. 1-bromobutane (>96%) and 1-methylpyrrolidine (>99%) were purchased from Sigma–Aldrich, LiTFSI (>99%; battery grade) from Ferro (USA).

A total of 68.5 g (0.5 mol) of 1-bromobutane (freshly distilled) was mixed with 42.6 g (0.5 mol) of 1-methylpyrrolidine in a flask with a reflux condenser. The mixture was stirred at 60 °C for 2 h to give a white solid. This solid was recrystallised from hot acetonitrile and dried for 5 h at 80 °C under vacuum to give white crystals (83 g; 75% yield). Compared to our previous synthesis [8], we lowered the reaction temperature from 80 to 60 °C with a noticeable improvement of the product purity. The temperature optimisation was previously recommended by Paulechka et al. for imidazolium-based ILs [35].

The substitution of bromide anion by $TFSI^-$ was performed in water, where $PYR_{14}TFSI$ is not soluble and forms hydrophobic globules at the bottom of the flask. The amount of 38.77 g (0.135 mol) of LiTFSI in 90 ml of water was added into a solution of 30.00 g (0.135 mol) $PYR_{14}Br$ in 60 ml of distilled water and stirred for 2 h at 70 °C and than overnight at room temperature. The arising phase of $PYR_{14}TFSI$ was removed and washed 6 times with 100 ml portions of distilled water and than 2 times with 100 ml portions of deionised water to remove LiBr. The absence of bromide anions was confirmed using the test with $AgNO_3$. The remaining water was evaporated under vacuum at 60 °C at a rotary evaporator.

According to Appetecchi et al. [36], $PYR_{14}TFSI$ was purified by treatment with alumina (Brockmann acidic I, Sigma–Aldrich) and active carbon (Darco G60, Sigma–Aldrich) in acetone (HPLC grade, Merck). After purification, the remaining acetone was evaporated under vacuum and pure $PYR_{14}TFSI$ was dried at 15 Pa and 90 °C for 24 h before stored in a dry argon-filled glove box ($[H_2O] < 1$ ppm; MBraun, USA). Yield: 43 g of colourless liquid (75.5%). The purity of dry ionic liquids was confirmed by NMR measured on Varian MERCURY 400 High Resolution NMR Spectrometer and results corresponded to our previous synthesis [8].

Lithium bis(fluorosulfonyl)imide (LiFSI) was synthesised according to the procedure published by Beran and Příhoda [37,38] and dried at 15 Pa and 65 °C for 20 h before stored in the glove box. Lithium bis(trifluoromethanesulfonyl)imide (battery grade) LiTFSI was purchased from Ferro (USA) and used as received. The electrolytes, 0.7 m LiTFSI and 0.7 m LiFSI were prepared by dissolving the selected salt in $PYR_{14}TFSI$ at ambient temperature in the glove box. The concentrations are expressed in molality (moles of the salt in 1 kg of solvent).

The TGA–DTA measurement was performed in argon flow at the heating rate of 5 °C min^{-1} with a Simultaneous Thermal Analysis Netzsch STA 409 (Germany).

2.2. Preparation of the electrodes and electrochemical tests

Electrode composites of graphite–carbon black (CB)–PVDF samples were prepared using SLP 30 or KS6L graphite (Timcal, Switzerland). The first one is described as Potato®-Shape graphite with surface area of 8 $m^2 g^{-1}$, while the latter displays high crystallinity and a higher specific area (20 $m^2 g^{-1}$). The composite consisted of 85% of graphite, 10 wt.% of carbon black (C-nergy™ Super C65, Timcal) and 5 wt.% of PVDF (M_n 534,000, Sigma–Aldrich) as a binder in 1-methyl-2-pyrrolidone (Sigma–Aldrich). The obtained slurry was cast onto a circular Cu foil with a diameter of 16 mm (2 cm^2). Before use, the electrodes with a loading between 2.5 and 3 mg cm^{-2} were dried in vacuum at 90 °C for at least 12 h.

2.3. Methods and equipment for the electrolyte characterisation

The potentio-galvanostats VMP3 (Bio-Logic, France) and PGSTAT 10 and 30 (Eco Chemie, The Netherlands) were used for electrochemical measurements.

The electrochemical properties were measured in ECC standard cells (EL-Cell, Germany) or in vacuum-sealed triplex foil (coffee bag foil) cells by using a Celgard® 2320 as a separator and a lithium foil as counter and reference electrodes. The galvanostatic measurements were performed at room temperature and at 55 °C with current density corresponding to C/10 in the potential range from 2 to 0 V vs. Li/Li^+. The slow scan-rate cyclic voltammetry was performed at 0.1 mV s^{-1} in the potential range from 2 to 0 V vs. Li/Li^+ at 55 °C.

EIS measurements were performed on symmetrical cells with two freshly rolled out lithium foils (geometric area 2 cm^2) separated with a Cellgard® 2500 separator and vacuum sealed in the triplex foil. In this study we used two different electrolytes (0.7 m LiFSI and 0.7 m LiTFSI in $PYR_{14}TFSI$). After assembling the symmetrical cells were immediately measured using the Hewlett Packard 4284A Precision LCR Meter in the frequency range 1 MHz to 20 Hz. Aged symmetrical cells were measured in the frequency range 65 kHz to 1 mHz, using the Solartron 1250A Frequency Response Analyser at room temperature with an amplitude of 10 mV.

Temperature dependent conductivity measurements were performed in the temperature range from 0 to 100 °C using a circulating bath Ministat 125-cc (precision of the temperature ±0.1 °C, Huber, Germany) and a conductivity cell (Jenway, platinum electrodes, cell constant $S = 1.00 \pm 0.01$). Using the FRA-2 module of the PGSTAT 30 potentiostat, a single potential impedance spectrum was measured in the frequency range from 10 kHz to 100 Hz. The obtained spectrum was analysed by the EcoChemie Autolab software producing the value of electrolyte resistivity.

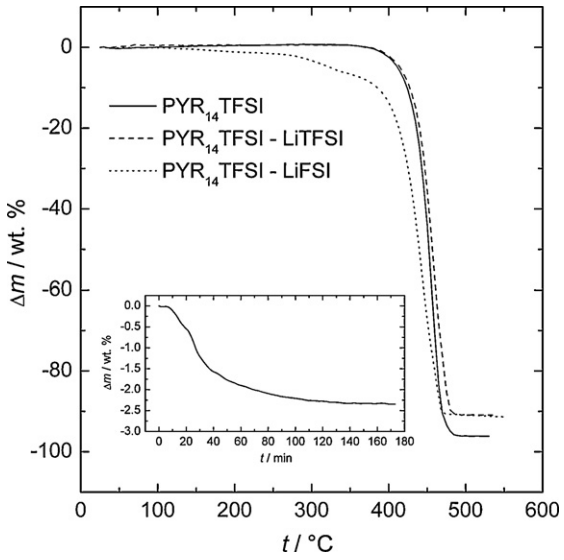

Fig. 1. TGA curves for neat $PYR_{14}TFSI$ and 0.7 m LiTFSI or LiFSI solutions in $PYR_{14}TFSI$ (5 °C min^{-1} heating rate, temperature range 30–550 °C; argon atmosphere), inserted: TGA curve of 0.7 m LiFSI in $PYR_{14}TFSI$ measured 170 min at constant temperature of 150 °C.

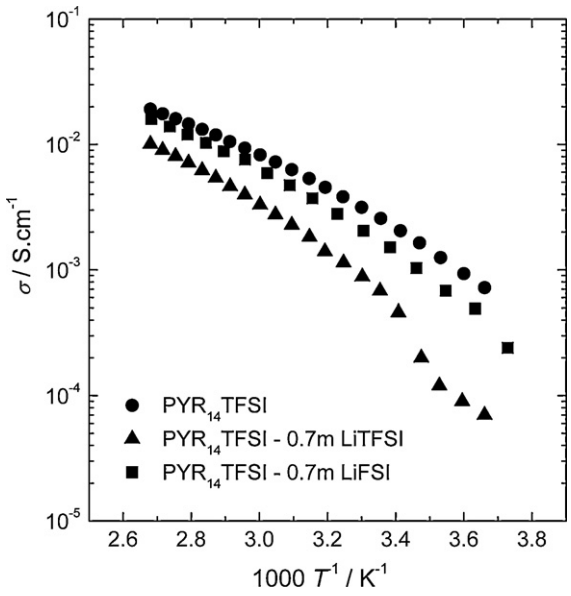

Fig. 2. Arrhenius plot for neat $PYR_{14}TFSI$ and 0.7 m LiTFSI or LiFSI solutions in $PYR_{14}TFSI$ (temperature range 0–100 °C).

3. Results and discussion

3.1. Thermal stability of the ionic liquid electrolytes

The thermal stability, nonflammability and incombustibility of pyrrolidinium-based ionic liquids are the key parameters from the safety point of view. Generally, the ionic liquids with FSI^- and $TFSI^-$ anion exhibit the highest thermal stability [28,39–41] and are much safer than the conventional carbonate-based electrolytes.

Fig. 1 presents the decomposition curves for studied $PYR_{14}TFSI$-based electrolytes, as measured by TGA. All samples have only minimal weight loss (less than 0.2 wt.%) below 120 °C. A noticeable loss (up to 5 wt.%) was observed above 200 °C in the case of LiFSI–$PYR_{14}TFSI$ electrolyte, while the neat $PYR_{14}TFSI$ remains stable up to 385 °C. In all cases, a single-step decomposition reaction occurs at rather high temperatures 350–480 °C.

The thermal stability of LiFSI–$PYR_{14}TFSI$ electrolyte can be affected by water traces, absorbed in the sample during the loading into the TGA analyser. It has been reported that the SO_2F group is more reactive towards water than SO_2CF_3, particularly at elevated temperatures [41], however the isothermal TGA showed no decomposition within 24 h at 125 °C [42]. We performed isothermal TGA of LiFSI–$PYR_{14}TFSI$ sample at 150 °C (shown in the inset of Fig. 1). Approximately 2.5 wt.% loss was observed during initial 80 min, but than the sample remained stable. This weight loss can be attributed to evaporation of water traces that were absorbed during sample loading and heating up.

3.2. Conductivity of ionic liquid electrolytes

The change of ionic conductivity with temperature was measured in the region from 0 to 100 °C and it is shown in Fig. 2. As expected, the conductivity of the lithium salt solutions in ionic liquids is lower that the conductivity of neat $PYR_{14}TFSI$. The dissolution of lithium salt in an ionic liquid leads to a system with a higher viscosity and a lower conductivity. Unlike in the carbonate-based electrolytes, where the conductivity maximum appears [43], the RTIL-based systems show a gradual decrease in conductivity in the whole range of salt concentration [44].

If we use LiFSI instead of LiTFSI, the conductivity decrease is not so deep there is not a substantial decrease in conductivity. The conductivities of 0.7 m LiTFSI and 0.7 m LiFSI in $PYR_{14}TFSI$ are 3.3 and 5.9 mS cm^{-1} at 60 °C, respectively. The LiFSI–$PYR_{14}TFSI$ electrolyte retains reasonable conductivity even at temperatures close to 0 °C. For LiTFSI-$PYR_{14}TFSI$ electrolyte we observed a reproducible and reversible drop of conductivity at ca. 15 °C, which is close to the temperature of the crystallisation process (formation of a new phase) observed by DSC in our previous paper [8].

The obtained data were fitted with the Vogel–Tamman–Fulcher (VTF) equation (in the logarithmic form):

$$\sigma T^{1/2} = A \ \exp\left[\frac{-E_A}{R(T-T_0)}\right] \quad (1)$$

where A is a parameter related to the number of charge carriers, E_A is the activation energy for conduction, R is the universal gas constant and T_0 the ideal glass transition temperature indicating the temperature at which the free volume extrapolates to zero. The analysis of the experimental conductivity data in terms of the VTF relationship leads to the determination of three empirical parameters: A, E_A and T_0, when T_0 is determined by fitting the experimental data with relationship (1).

3.3. Electrochemical impedance spectroscopy

Formation of the passive layer (ageing) on the lithium foil was studied in symmetrical cells at open circuit conditions. With the aim to follow fast changes in the starting period after assembling the cells we first measured the dynamic interface impedance behaviour using impedance spectroscopy in the frequency range from 1 MHz to 20 Hz. Fig. 3 shows the evolution of the EIS spectra of the symmetrical Li|$PYR_{14}TFSI$–0.7 m LiFSI|Li cell during the first hours after cell assembly. A well-developed high-frequency impedance arc (H.F.-arc) can be observed. The time evolution of the EIS spectra during "ageing" demonstrates the dynamic nature of the transport properties in the cell during the first few minutes. This can be more clearly followed if we plot the resistance of the high-frequency arc ($R_{H.F.}$-arc) vs. time of "ageing" (inset in Fig. 3). A similar dynamic behaviour was also observed in the case of the symmetrical cells comprising the $PYR_{14}TFSI$–0.7 m LiTFSI electrolyte.

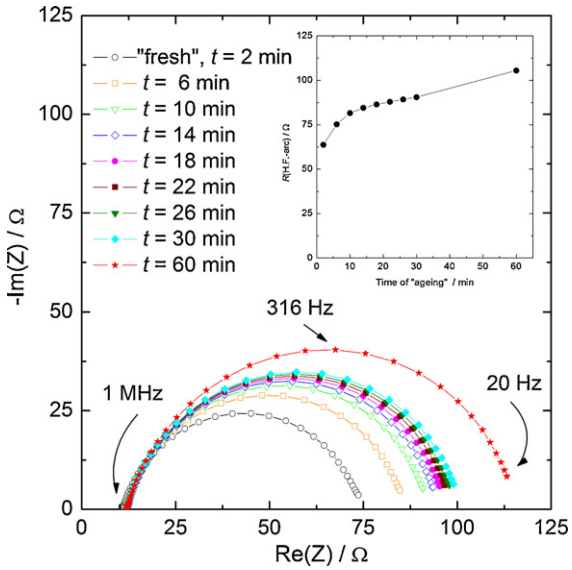

Fig. 3. Time evolution of the EIS spectra of the symmetrical Li|$PYR_{14}TFSI$–0.7 m LiFSI|Li cell during the first hour after cell assembly; inset: time evolution of the resistance of the high-frequency arc with time from cell assembly. All measurements were performed at 25 °C.

The set of impedance spectra shown in Fig. 3 clearly demonstrates the dynamics of the initial rapid changes when a fresh lithium surface was exposed to ionic liquids based electrolytes used in our experiments. Similar dynamics was observed in the work of Scrosati and coworkers [45]. The present observation demonstrates the importance of time delay after symmetrical cell was assembled and measured. In our experiment (Fig. 3) one frequency sweep was accomplished in 40 s. In general it might be questionable the accuracy of the data (capacitances, resistances) obtained by the deconvolution of the impedance spectra of the "fresh" cells that were possibly measured in the immoderately broad frequency ranges (i.e. rather long times for the EIS frequency sweep).

Symmetrical cells were left under open circuit conditions at room temperature and we measured EIS responses after 3 and 24 days of ageing in the frequency range 65 kHz to 1 mHz as shown in Fig. 4. The cell comprising the LiFSI salt clearly exhibits lower impedances than the cell comprising the LiTFSI salt. The resistances of the high-frequency arc measured after 3 and 24 days of ageing are: 322 Ω and 1244 Ω (for 0.7 m LiFSI), 710 Ω and 1740 Ω (for 0.7 m LiTFSI), respectively. Note that the EIS responses obtained after 24 days of ageing in the medium-frequency region (starting at 0.1 Hz and lower) do not exhibit the typical arc shape but rather an inclined line possibly indicating a diffusion phenomena. The values

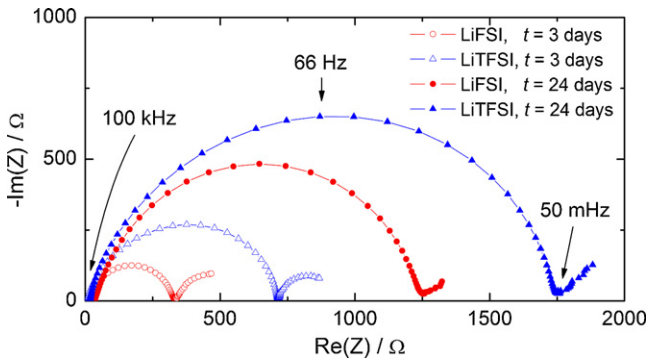

Fig. 4. EIS spectra of the symmetrical Li|electrolyte|Li cells containing 0.7 m LiFSI or 0.7 m LiTFSI in $PYR_{14}TFSI$ obtained after 3 days and 24 days of ageing. All measurements were performed at 25 °C.

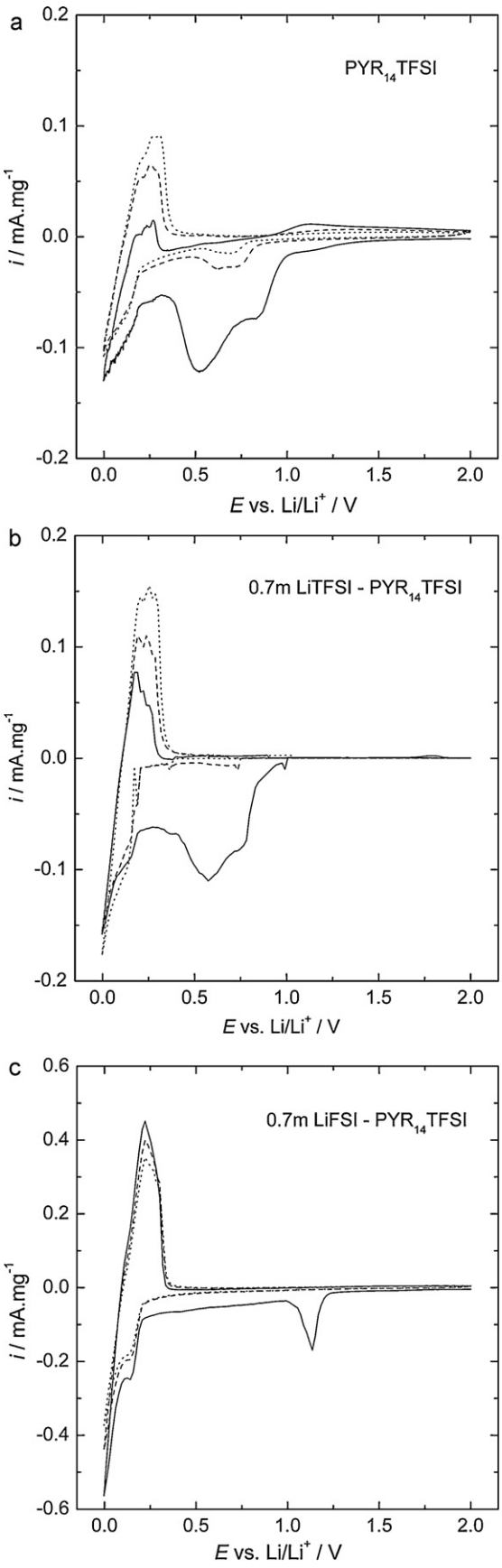

Fig. 5. Initial cyclic voltammograms of graphite composite electrode KS6L-C65-PVDF (85–10^{-5} wt.%) in (A) neat $PYR_{14}TFSI$, (B) 0.7 m LiTFSI–$PYR_{14}TFSI$, (C) 0.7 m LiFSI–$PYR_{14}TFSI$ (cycle 1 – full line, cycle 2 – dash line, cycle 3 – dot line). Conditions: 0.1 mV s^{-1}, 55 °C, counter and reference metal lithium.

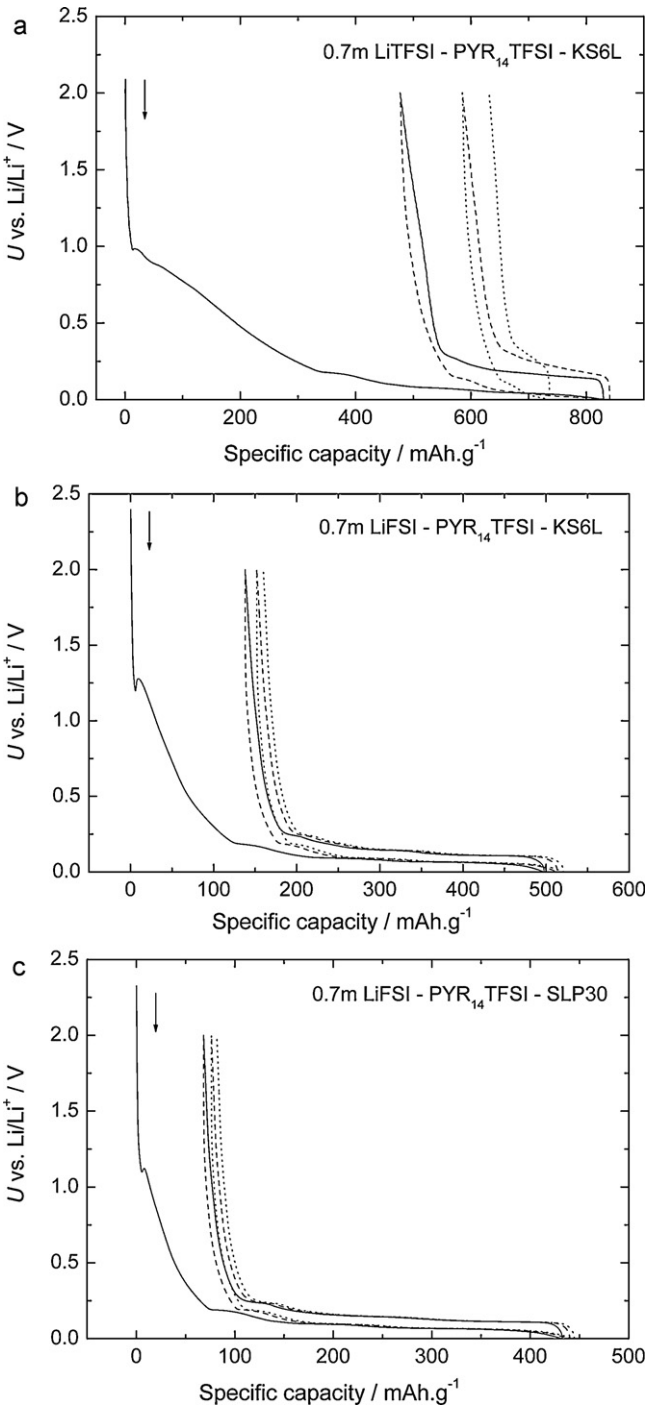

Fig. 6. The initial discharge-charge profiles of the half-cell Li|0.7 m LiTFSI-$PYR_{14}TFSI$|graphite KS6L (A) and half-cells Li|0.7 m LiFSI–$PYR_{14}TFSI$|graphite KS6L (B) and SLP30 (C) at 55 °C with current density corresponding to C/10.

of the resistances of the high-frequency part contribution for 0.7 m LiFSI seem to be in the same range as reported by Lewandowski and Świderska-Mocek [20] and in that way an order of magnitude (favorably) lower than in the case of a system similar to the present one previously studied by Scrosati and coworkers [45]. Considering these results, we can conclude that evolution of the impedance response is very similar for both salts used in the study, lower values obtained for the cell comprising the LiFSI salt indicate lower transport restraints in the corresponding electrochemical (insertion material holding) cell.

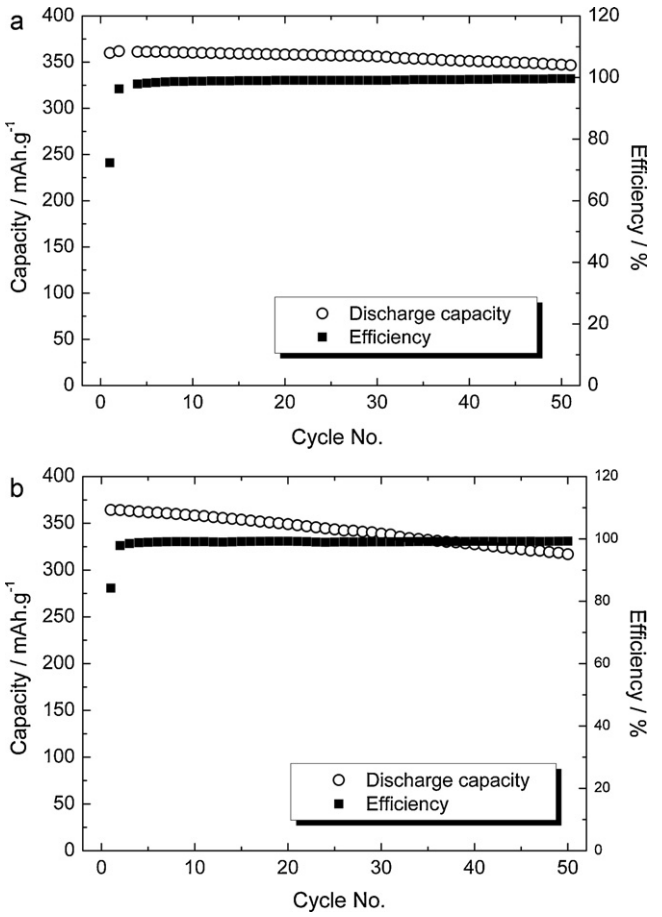

Fig. 7. Cycle performance of (A) KS6L and (B) SLP30 graphite composite electrodes in 0.7 m LiFSI–$PYR_{14}TFSI$ electrolyte at 55 °C with current density corresponding to C/10.

3.4. Cyclic voltammetry of graphite in ionic liquid electrolytes

The lithium intercalation process was studied on composite electrodes consisting of graphite (active material), carbon black (spacer and electronic conductor) and PVDF (binder). Fig. 5 presents the initial cyclic voltammograms (CVs) of KS6L graphite electrode in three different electrolytes: neat $PYR_{14}TFSI$, 0.7 m LiTFSI in $PYR_{14}TFSI$ and 0.7 m LiFSI in $PYR_{14}TFSI$. The CVs were measured at 55 °C and 0.1 mV s^{-1} scan rate.

On noble electrodes such as platinum or gold, no electrochemical reduction of $PYR_{14}TFSI$ appears until 0 V vs. Li/Li^+, which indicates much higher electrochemical stability of $PYR_{14}TFSI$ compared to imidazolium-based compounds [30]. A good electrochemical stability of $PYR_{14}TFSI$ in the considered potential region was also confirmed by in situ FTIR [46,47]. Fig. 5a shows the cyclic voltammogram of neat $PYR_{14}TFSI$. Broad cathodic peaks at 0.9 and 0.5 V can be attributed to intercalation of PYR_{14}^+ cations into the graphite structure that is partially reversible (see an anodic peak at c. 1.2 V on the first cycle). We also observed a small peak of the Li^+ intercalation–deintercalation process probably due to the presence of Li^+ released from the lithium metal counter electrode. In the subsequent scans, the Li^+ deintercalation peak increases together with the decrease of PYR_{14}^+ intercalation and deintercalation. Hence, a ternary intercalation compound $Li_X(PYR_{14})_YC_Z$ is probably formed with progressive change in the composition [48].

The LiTFSI-$PYR_{14}TFSI$ electrolyte (Fig. 5b) shows poor electrochemical performance and high irreversibility of the Li^+ intercalation–deintercalation process and rapid fading of the

Table 1
Specific conductivities (at 20 and 60 °C), apparent activation energy E_A from the fit by VTF equation and the start decomposition temperatures (T_{dec}) determined by TGA of studied electrolytes.

Electrolyte	σ (20 °C) (mS cm^{-1})	σ (60 °C) (mS cm^{-1})	E_A (kJ mol^{-1})	T_{dec} (°C)
$PYR_{14}TFSI$	2.1	8.3	6.9	385
$PYR_{14}TFSI$–0.7 m LiTFSI	0.5	3.3	6.7	390
$PYR_{14}TFSI$–0.7 m LiFSI	1.5	5.9	6.8	205

Table 2
Discharge capacities and coulombic efficiencies for the first three charge–discharge cycles at C/10 rate and 55 °C (0.7 m salt concentration).

Electrolyte	Graphite	Discharge capacity (mAh g^{-1})			Coulombic efficiency (%)		
		1st	2nd	3rd	1st	2nd	3rd
LiTFSI–$PYR_{14}TFSI$	KS6L	353	256	105	42.5	70.3	69.5
LiFSI–$PYR_{14}TFSI$	KS6L	360	362	361	72.3	96.3	97.9
LiFSI–$PYR_{14}TFSI$	SLP30	364	364	363	84.2	97.9	98.5

capacity. The irreversible reduction peak appears below 1 V vs. Li/Li$^+$ similarly to the system described above.

When LiFSI was used as an electrolyte component, the behaviour of graphite was different (Fig. 5c). The irreversible reduction occurs in the potential region from 1.3 to 0.25 V, followed by a reversible lithium intercalation into graphite below 0.2 V. Such a desirable, reversible behaviour is due to the electrochemical reduction of the FSI^- anion during the first cycle. Cyclic voltammetry illustrates that the film formation is finished during the first cycle. In the second and consequent cycles, no electrochemical reduction is visible any more, indicating that the filming process is completed. Accomplished SEI film formation on the graphite during first reduction cannot be compared with a time evolution of impedance increase measured on lithium foil by EIS. Influence of graphite ageing in the contact with ionic liquids need to be measured in the future to estimate potential commercial use.

3.5. Galvanostatic measurements in Li/graphite half-cells

The galvanostatic measurements of graphite composite electrodes were performed at 55 °C with current density corresponding to C/10 rate. The initial three charge–discharge curves of the Li/KS6L graphite cell with LiTFSI-$PYR_{14}TFSI$ electrolytes are given in Fig. 6a. During the first charge, a large irreversible capacity was observed at potentials 1–0.25 V vs. Li/Li$^+$, that corresponds to the reduction waves in Fig. 5a and b (intercalation of PYR_{14}^+ cation). Subsequently, we observed a plateau characteristic of Li$^+$ intercalation. The discharge capacity of the Li$^+$ deintercalation in the first cycle was relatively high (353 mAh g^{-1}), but rapidly decreased in the second and following cycles. The coulombic efficiencies during the first three cycles were 42.5, 70.3 and 69.5%, respectively. This result showed an unstable electrochemical environment for the lithium intercalation in graphite when the LiTFSI-$PYR_{14}TFSI$ electrolyte was used (Table 1).

The cycling properties of KS6L and SLP30 graphite in LiFSI–$PYR_{14}TFSI$ are plotted in Fig. 6b and c. As it can be distinguished from the initial three cycles, the presence of LiFSI in the electrolyte strongly changes the electrochemical behaviour of graphite. The onset of the SEI formation during the first cycle is consistent with the cathodic peak and wave position obtained in Fig. 5c. After mild reduction decomposition of the FSI^- anion, the cell voltage rapidly dropped in the voltage region of lithium intercalation into graphite.

According to the shape of charge and discharge curves, the intercalation/deintercalation process proceeded through different stages, identical to a typical electrolyte system such as 1 M $LiPF_6$–DEC–EC. The stability of LiFSI–$PYR_{14}TFSI$ electrolyte was comparable with a standard carbonate-based electrolyte. Based on the presented results, we can conclude, that the SEI formed during the first cycle is a stable, electron insulating and lithium ion conducting film.

The discharge capacities and coulombic efficiencies achieved during the first three cycles are summarised in Table 2. As it can be seen, in the KS6L graphite with a higher surface area, the coulombic efficiency in the first charge–discharge is lower than in SLP30 graphite, which indicates a higher consumption of SEI-forming agent (FSI^- anion) for the formation of SEI. In both cases 99.5–99.8% efficiency is reached after a short time.

KS6L graphite shows a good cycling stability (Fig. 7) in the 0.7 m LiFSI–$PYR_{14}TFSI$ electrolyte achieving the capacity of 350–360 mAh g^{-1}, while SLP30 graphite exhibits a slight fading from 364 to 317 mAh g^{-1} within 50 cycles.

4. Conclusions

In this paper we have reported the results obtained by using LiFSI–$PYR_{14}TFSI$ electrolyte in combination with two types of graphite (KS6L and SLP30) at an elevated temperature of 55 °C. The 0.7 m LiFSI solution in $PYR_{14}TFSI$ exhibits a good ionic conductivity (5.9 mS cm^{-1} at 55 °C), nonflammability and high thermal stability. The use of LiFSI–$PYR_{14}TFSI$ showed high electrochemical stability of the ionic liquid during lithium intercalation into graphite due to the ability of the FSI^- anion to establish the SEI in the formation cycles. When used in combination with KS6L graphite, the studied system shows high performance in terms of specific capacity (350–360 mAh g^{-1}) and cycling efficiency (99.5–99.8%).

Acknowledgements

This research was supported by the Academy of Sciences (AV0Z40320502), the Grant Agency of the Academy of Sciences of the Czech Republic (KJB200320801 and KJB200320901), by the Ministry of Education, Youth and Sports, Czech Republic (LC523), by the financial support from the Ministry of Education, Science and Sport of Slovenia, by the Slovenian Research Agency and by the CO-NOT centre of excellence. We thank Timcal for supplying graphite and carbon black.

References

[1] B. Ravdel, K.M. Abraham, R. Gitzendanner, J. DiCarlo, B. Luch, C. Campion, J. Power Sources 119–121 (2003) 805–1805.
[2] H. Yang, G.V. Zhuang, P.N. Ross, J. Power Sources 161 (2006) 573.
[3] M. Armand, F. Endres, D.R. MacFarlane, H. Ohno, B. Scrosati, Nat. Mater. 8 (2009) 621–629.
[4] M. Galinski, A. Lewandowski, I. Stepniak, Electrochim. Acta 51 (2006) 5567–5580.

[5] H. Nakagawa, Y. Fujino, S. Kozono, Y. Katayama, T. Nukuda, H. Sakaebe, H. Matsumoto, K. Tatsumi, J. Power Sources 174 (2007) 1021–1026.
[6] H.H. Zheng, H.C. Zhang, Y.B. Fu, T. Abe, Z. Ogumi, J. Phys. Chem. B 109 (2005) 13676–13684.
[7] A.P. Lewandowski, A.F. Hollenkamp, S.W. Donne, A.S. Best, J. Power Sources 195 (2010) 2029–2035.
[8] M. Nádherná, R. Dominko, D. Hanzel, J. Reiter, M. Gabersček, J. Electrochem. Soc. 156 (2009) A619–A626.
[9] I.A. Profatilova, N.S. Choi, S.W. Roh, S.S. Kim, J. Power Sources 192 (2009) 636–643.
[10] B. García, S. Lavallee, G. Perron, C. Michot, M. Armand, Electrochim. Acta 49 (2004) 4583.
[11] F.F.C. Bazito, Y. Kawano, R.M. Torresi, Electrochim. Acta 52 (2007) 6427–6437.
[12] T.E. Sutto, J. Electrochem. Soc. 154 (2007) P130–P135.
[13] M. Nádherná, R. Dominko, M. Gabersček, J. Reiter, 216th Meeting of the Electrochemical Society, Wien, Austria, October 4–9, 2009 (abstract 519).
[14] Y. Katayama, M. Yukumoto, T. Miura, Electrochem. Solid-State Lett. 5 (2003) A96–A97.
[15] T. Sato, T. Maruo, S. Marukane, K. Takagi, J. Power Sources 138 (2004) 253–261.
[16] H. Sano, H. Sakaebe, H. Matsumoto, 216th Meeting of the Electrochemical Society, Wien, Austria, October 4–9, 2009 (abstract 664).
[17] P.C. Howlett, D.R. MacFarlane, A.F. Hollenkamp, Electrochem. Solid State Lett. 7 (2004) A97–A101.
[18] T.E. Sutto, T.T. Duncan, T.C. Wong, Electrochim. Acta 54 (2009) 5648–5655.
[19] M. Holzapfel, C. Jost, A. Prodi-Schwab, F. Krumeich, A. Würsig, H. Buqa, P. Novák, Carbon 43 (2005) 1488–1498.
[20] A. Lewandowski, A. Świderska-Mocek, J. Power Sources 194 (2009) 502–507.
[21] G.H. Lane, A.S. Best, D.R. MacFarlane, M. Forsyth, A.F. Hollenkamp, Electrochim. Acta 55 (2010) 2210–2215.
[22] Y.B. Fu, C. Chen, C.C. Qiu, X.H. Ma, J. Appl. Electrochem. 39 (2009) 2597–2603.
[23] H. Zheng, B. Li, Y. Fu, T. Abe, Z. Ogumi, Electrochim. Acta 52 (2006) 1556–1562.
[24] H. Zheng, K. Jiang, T. Abe, Z. Ogumi, Carbon 44 (2006) 203–210.
[25] K. Zaghib, P. Charest, A. Guerfi, J. Shim, M. Perrier, K. Striebel, J. Power Sources 134 (2004) 124–129.
[26] K. Zaghib, P. Charest, A. Guerfi, J. Shim, M. Perrier, K. Striebel, J. Power Sources 146 (2005) 380–385.
[27] C. Michot, M. Armand, M. Gauthier, N. Ravet, Can. Patent WO9940025-A (1999).
[28] M. Ishikawa, T. Sugimoto, M. Kikuta, E. Ishiko, M. Kono, J. Power Sources 162 (2006) 658–662.
[29] S. Seki, Y. Kobayashi, H. Miayshiro, Y Ohno, Y. Mita, N. Terada, P. Charest, A. Guerfi, K. Zaghib, J. Phys. Chem. C 112 (2008) 16708–16713.
[30] T. Sugimoto, M. Kikuta, E. Ishiko, M. Kono, M. Ishikawa, J. Power Sources 183 (2008) 436–440.
[31] A. Guerfi, S. Duchesne, Y. Kobayashi, A. Vijh, K. Zaghib, J. Power Sources 175 (2008) 866–873.
[32] G.B. Appetecchi, M. Montanino, A. Balducci, S.F. Lux, M. Winter, S. Passerini, J. Power Sources 192 (2009) 599–605.
[33] S.F. Lux, M. Schnuck, G.B. Appetecchi, S. Passerini, M. Winter, A. Balducci, J. Power Sources 192 (2009) 606–611.
[34] Y.D. Wang, K. Zaghib, A. Guerfi, F.F.C. Bazito, R.M. Torresi, J.R. Dahn, Electrochim. Acta 52 (2007) 6346–6352.
[35] Y.U. Paulechka, G.J. Gabo, A.V. Blokhin, A.S. Shaplov, E.I. Lozinskaya, Ya.S. Vygodskii, J. Chem. Thermodyn. 39 (2007) 158–166.
[36] G.B. Appetecchi, S. Scaccia, C. Tizzani, F. Alessandrini, S. Passerini, J. Electrochem. Soc. 153 (2006) A1685–A1691.
[37] M. Beran, J. Příhoda, Z. Anorg, Allg. Chem. 631 (2005) 55–59.
[38] M. Beran, J. Příhoda, Z. Žák, M. Černík, Polyhedron 25 (2006) 1292–1298.
[39] J. Huang, A.F. Hollenkamp, J. Phys. Chem. C 114 (2010) 21840–21847.
[40] A.S. Best, A.I. Bhatt, A.F. Hollenkamp, J. Electrochem. Soc. 157 (2010) A903–A911.
[41] E. Paillard, Q. Zhou, W.A. Henderson, G.B. Appetecchi, M. Montanino, S. Passerini, J. Electrochem. Soc. 156 (2009) A891–A895.
[42] Q. Zhou, W.A. Henderson, G.B. Appetecchi, M. Montanino, S. Passerini, J. Phys. Chem. B 112 (2008) 13577–13580.
[43] M.S. Ding, T.R. Jow, J. Electrochem. Soc. 151 (2004) 2007–2015.
[44] S. Seki, Y. Ohno, Y. Kobayashi, H. Miyashiro, A. Usami, Y. Mita, H. Tokuda, M. Watanabe, K. Hayamizu, S. Tsuzuki, J. Electrochem. Soc. 154 (2007) A173–A177.
[45] A. Fernicola, F. Croce, B. Scrosati, T. Watanabe, H. Ohno, J. Power Sources 174 (2007) 342–348.
[46] S.F. Lux, M. Schmuck, S. Jeong, S. Passerini, M. Winter, A. Balducci, Int. J. Energy Res. 34 (2010) 97–106.
[47] A. Balducci, M. Schmuck, W. Kern, B. Rupp, S. Passerini, M. Winter, ECS Trans. 11 (2008) 109–114.
[48] E. Markevich, V. Baranchugov, G. Salitra, D. Aurbach, M.A. Schmidt, J. Electrochem. Soc. 155 (2008) A132–A137.